LIMNOLOGY
and
OCEANOGRAPHY

ASLO

Limnol. Oceanogr. 63, 2018, 431–444

doi: 10.1002/lno.10641

Effect of settled diatom-aggregates on benthic nitrogen cycling

Ugo Marzocchi,[1,2,3]* **Bo Thamdrup**,[1] **Peter Stief**,[1] **Ronnie N. Glud**[1,4]

[1]Department of Biology and Nordic Center for Earth Evolution (NordCEE), University of Southern Denmark, Odense M, Denmark
[2]Department of Analytical, Environmental and Geo-Chemistry, Vrije Universiteit Brussel (VUB), Brussels, Belgium
[3]Center for Geomicrobiology and Section for Microbiology, Aarhus University, Aarhus, Denmark
[4]Scottish Association for Marine Science, Oban, United Kingdom

Abstract

The marine sediment hosts a mosaic of microhabitats. Recently it has been demonstrated that the settlement of phycodetrital aggregates can induce local changes in the benthic O_2 distribution due to confined enrichment of organic material and alteration of the diffusional transport. Here, we show how this microscale O_2 shift substantially affects benthic nitrogen cycling. In sediment incubations, the settlement of diatom-aggregates markedly enhanced benthic O_2 and NO_3^- consumption and stimulated NO_2^- and NH_4^+ production. Oxygen microprofiles revealed the rapid development of anoxic niches within and underneath the aggregates. During 120 h following the settling of the aggregates, denitrification of NO_3^- from the overlying water increased from 13.5 μmol m^{-2} h^{-1} to 24.3 μmol m^{-2} h^{-1}, as quantified by ^{15}N enrichment experiment. Simultaneously, N_2 production from coupled nitrification-denitrification decreased from 33.4 μmol m^{-2} h^{-1} to 25.9 μmol m^{-2} h^{-1}, probably due to temporary inhibition of the benthic nitrifying community. The two effects were of similar magnitude and left the total N_2 production almost unaltered. At the aggregate surface, nitrification was, conversely, very efficient in oxidizing NH_4^+ liberated by mineralization of the aggregates. The produced NO_3^- was preferentially released into the overlying water and only a minor fraction contributed to denitrification activity. Overall, our data indicate that the abrupt change in O_2 microdistribution caused by aggregates stimulates denitrification of NO_3^- from the overlying water, and loosens the coupling between benthic nitrification and denitrification both in time and space. The study contributes to expanding the conceptual and quantitative understanding of how nitrogen cycling is regulated in dynamic benthic environments.

The seafloor is of key importance for the removal of reactive nitrogen from the oceans (e.g., Seitzinger et al. 2006; Eugster and Gruber 2012). Here, the reduction of soluble inorganic nitrogen species (i.e., NO_3^-, NO_2^-) to gaseous NO, N_2O, and N_2 by denitrification occurs in the anoxic zone underlying the oxic sediment layer that blankets the seafloor. Numerous investigations have documented that the O_2 distribution in the sediment exhibits high vertical and horizontal heterogeneity. Within the milli- to centimeter scale, O_2 consumption rates can vary over an order of magnitude, generating a mosaic of oxic to hypoxic/anoxic niches (e.g., Rabouille et al. 2003; Glud et al. 2005, 2009). This small-scale spatial (and temporal) heterogeneity has traditionally been linked to the activity of benthic fauna or to the deposition of fecal pellets. Settling algae-aggregates have only recently been proposed to induce temporary O_2 depleted areas on the sediment surface (Boetius et al. 2013; Glud et al. 2014), and thereby generate anoxic microsites suitable for denitrification (Lehto et al. 2014). To date, however, the development and the importance of these transient microniches for benthic nitrogen cycling have not been experimentally investigated.

Sinking aggregates and fecal pellets represent a major pathway for transporting material from the surface to the deep ocean and the underlying benthic environment. Aggregates are generated when cells and particles collide and adhere, and preferentially form in the photic zone in the wake of phytoplankton blooms (Thornton 2002), or by sea-ice algae in the spring during intense ice melting periods (Glud et al. 2014). Phycodetrital aggregates are quickly colonized by prokaryotic organisms (Kiorboe et al. 2002) and, with a delay, also by eukaryotes (Ploug and Grossart 2000; Worner et al. 2000), which together constitute an aggregate-

*Correspondence: ugo.marzocchi@bios.au.dk

associated food-web ultimately based on aggregate biomass mineralization. Depending on size, ambient O_2 levels, and temperature, sinking aggregates may develop an anoxic center due to the high inherent mineralization rates sustained by the degradation of the labile algal biomass (Ploug and Grossart 1999, 2000) and to O_2 diffusion limitation (Alldredge and Cohen 1987; Ploug et al. 1997). Such internal anoxia have been shown to stimulate dissimilatory reduction of NO_3^- from the surrounding water, both in cyanobacterial and diatom aggregates, leading primarily to the release of NH_4^+, NO_2^-, and N_2 back into the surrounding water (Klawonn et al. 2015; Stief et al. 2016). Mineralization of algal biomass may also contribute to the net release of NH_4^+ from sinking aggregates (Klawonn et al. 2015; Ploug and Bergkvist 2015). Additionally, several diatom species have the ability to accumulate NO_3^- intracellularly to sustain dissimilatory anaerobic metabolism (Lomas and Glibert 2000; Seitzinger et al. 2006; Kamp et al. 2011, 2013), this may further stimulate nitrogen reducing pathways in sinking aggregates (Kamp et al. 2016; Stief et al. 2016).

It is to be expected that intensified aggregate-associated nitrogen cycling will prevail after the settlement at the seafloor. To date, it remains elusive, however, whether and how benthic nitrogen cycling might be affected by the complex microscale interaction between aggregates and sediment (Lehto et al. 2014). To improve our quantitative and mechanistic understanding on the interplay between sediment and settled aggregates, we studied the microscale O_2 dynamics within and around freshly deposited phycodetrital aggregates, and how this affected benthic denitrification and the exchange of O_2 and dissolved inorganic nitrogen (DIN, i.e., NO_3^-, NO_2^-, and NH_4^+) for up to 7 d in a flow-through system. Moreover, the contribution of aggregate-bound N to the DIN exchange, nitrification and denitrification rates was quantified by selectively labeling the aggregate biomass with ^{15}N isotopes.

Methods

Aggregate production and sediment sampling

For the production of phycodetrital aggregates, *Skeletonema marinoi* (CCMP1332, NCMA) was cultured using F/2 medium plus silicate (Guillard and Ryther 1962). Diatom-aggregates were formed in 550 mL bottles filled with 50 mL of stationary-phase *S. marinoi* culture and natural seawater (salinity 30‰). The bottles were rotated on a plankton wheel for 3–4 d (16°C, light:dark cycle 14:10 h) until aggregates (2–5 mm diameter) formed (Stief et al. 2016). At 2-day intervals, one third of the seawater in each bottle was replaced with fresh seawater to maintain the O_2 level at $>80\%$ air-saturation (AS) and avoid accumulation of waste products from the growing *S. marinoi* culture.

Coastal sediment was collected north of Ven (Sweden) (55°58′334 N; 12°41′594 E) at 32 m depth (bottom water temp. 10°C, salinity 35‰) by repeated casts of an HAPS corer (Kanneworff and Nicolaisen 1972). The sediment was then subsampled using cylindrical Plexiglas® core liners (i.d. × height 5 × 20 cm), and transported to the laboratory. Within a few hours, large macrofauna, exclusively represented by Ophiuroids, was removed using forceps and the cores were transferred into a tank with stirred artificial seawater (30‰; Seasalt, Tetra. NO_3^- concentration approx. 5 μM) at 16°C, in the dark. Sediment cores exhibiting a relatively homogeneous O_2 penetration depth (typically 4–5 mm) were selected for the experiments.

Aggregate and sediment characterization

For characterization, 3- to 5-day-old aggregates were extracted from the production bottles using a glass tube (i.d. 8 mm) connected to a syringe that allowed the retrieval of single aggregates with minimal disturbance. Aggregates were then transferred onto a Petri dish containing artificial seawater (30‰) to wash off the residual growth medium still present in the aggregate-production bottles, and to photograph the aggregates. The three-axis of the ellipsoidal aggregates were measured by processing the images with the freely available software ImageJ (http://imagej.nih.gov). Dry weight and organic matter content (OM) (measured as loss on ignition, LOI) were measured after drying a batch of 16 randomly selected aggregates at 65°C (for 24 h) and 520°C (for 5 h), respectively.

The amount of particulate organic carbon (POC) delivered to the sediment as aggregate biomass was calculated by the volumetric LOI multiplied by the total volume of aggregates added on each experiment and corrected by 0.4 (fraction of C in a CH_2O molecule as m.w.). Particulate organic nitrogen (PON) was calculated by the POC content (mol) and the C : N ratio of the aggregates.

To determine the content of intracellular nitrate ($ICNO_3$) according to Kamp et al. (2016), aggregates were sized as described above and transferred into pre-weighed centrifugation tubes containing 0.5 mL of seawater. The tubes were then re-weighed, snap-frozen using liquid nitrogen, and stored at −20°C. Samples were exposed to three freeze-thaw cycles to promote cell-lysis and vortexed for 20 s. An aliquot of the homogeneous solution was then measured for NO_3^- using the V^{3+} chemoluminesence method described below. The $ICNO_3$ pool was determined as the difference between the amount of NO_3^- in the sample and in a control with only seawater. As the $ICNO_3$ determination requires a destructive procedure, the initial $ICNO_3$ of the aggregates used for the incubations was calculated from the relation between the aggregate volume and the volumetric $ICNO_3$ concentration determined on 25, randomly selected, aggregates from the aggregate-production bottles. At the end of each flow-through incubation, aggregates were carefully removed from the sediment, sized, and the $ICNO_3$ was determined as described above. $ICNO_3$ loss throughout the incubation was obtained from the difference between the final and the initial $ICNO_3$ pool size.

Sediment porosity (vol : vol) and OM content (as LOI) was determined as above at a depth resolution of 5 mm.

Oxygen microprofiles

The influence of settled diatom-aggregates on the benthic O_2 micro-distribution was assessed by O_2 microsensor profiles. Three aggregates were randomly extracted from the production bottles and positioned on intact sediment cores. Sediment and aggregates were kept in the dark in an aquarium with artificial seawater (30‰) at the experimental temperature of 16°C. The water was constantly flushed with a mixture of air and N_2 to maintain the O_2 concentration at 70% (AS), which is representative of prevailing bottom water O_2 level in temperate and tropical regions (i.e., 61% of seafloor area with O_2 level between 55% and 85% AS, calculated from Schlitzer, R., Ocean Data View, http://odv.awi.de, 2016). To minimize the buildup of a thick diffusive boundary layer that would impose an O_2 transport limitation at the sediment water interface (Rasmussen and Jorgensen 1992), the water was kept mixed by rotating magnetic bars driven by an external motor (24 r.p.m.). Oxygen microprofiles were measured daily through the center of the aggregates, and on two occasions (at 76 h and 168 h), a transect (1 mm interval) was measured across an aggregate. For comparison, a similar transect was measured on the bare sediment before positioning the aggregate. Microprofiles were measured with an O_2 microsensor constructed and calibrated according to Revsbech (1989). The sensor cathode was polarized at +0.8 V, and the signal was read on a custom-made picoammeter connected via a data acquisition system (AD216, Unisense, Denmark) to a computer. The sensor was mounted on a motor-driven micromanipulator that allowed for profiling at 50 μm vertical steps. The sensor tip was manually positioned at the sediment/aggregate surface while observing it through a horizontal dissection microscope.

The sediment anoxic volume induced by the presence of the aggregates at 76 h of incubation was estimated as the sum of the volumes of truncated ellipsoidal cones spanning between the sediment surface and the depth of O_2 penetration before the addition of the aggregates (i.e., 4.8 mm). The proportions between the radii of the aggregates and the upper and lower cone surfaces, respectively, were approximated using Fig. 2d (76 h). Thus, the top surface area was set equal to the anoxic footprint of each aggregate on the sediment surface and calculated using the 30% of each aggregate radii length. The base was calculated using the 180% of each aggregate radii length. This calculation provides a maximum estimation as it assumes that all aggregates induce an anoxic cone.

Flow-through incubation I – ^{15}N-labeled NO_3^- in overlying water

In parallel to the O_2 micro-distribution measurements on single aggregates, the integrated effect of the settlement of 11 aggregates on: (1) benthic O_2 consumption, (2) DIN exchange, (3) denitrification, and (4) $ICNO_3^-$ release was investigated on sediment cores incubated in a flow-through system (Fig. 1). This enabled ^{15}N enrichment experiments while maintaining constant O_2 level in the overlying water over periods of days or weeks.

Two sediment cores were placed into cylindrical glass chambers (i.d. × height 5.4 × 16 cm). The sediment surface was positioned at about 3.5 cm below the upper rim. The top of each chamber was then sealed with a gas-tight glass lid, thereby enclosing a water volume of ca. 60 mL above the sediment without leaving a headspace. Two openings situated diametrically at 1 cm below the upper rim allowed to connect the water-filled compartment of each chamber, in parallel, to the flow-through system. Artificial seawater, amended with 30 μM $^{15}NO_3^-$ (98 atom% ^{15}N; Sigma-Aldrich) and with a background concentration of 5 μM NO_3^-, was fed from a reservoir (10 L) through the incubation chambers at constant rates of 0.14–0.18 mL min^{-1} in chamber 1 and 2, respectively with peristaltic pumps (Ole Dich, Denmark). At these rates, the average retention time of water within the chambers amounted to 5–7 h. Suspended magnetic stirring bars driven by an external motor (24 r.p.m.) ensured homogeneous water mixing inside the chambers. The O_2 level in both chambers was maintained at 70% AS by flushing the reservoir with a mixture of air (90%) and O_2 (10%). Oxygen levels in the reservoir and inside each chamber were constantly monitored by fiber-optic O_2 sensors connected to an O_2-reader (PyroScience, Germany). All sediment incubations were performed in darkness at 16°C.

After an acclimation period of 7 d with continuous flow-through, monitoring of the concentration and isotopic composition of NO_x^-, NO_2^-, NH_4^+, and N_2 began by sampling water at the inlet and outlet of each chamber (once or twice per day) during the following 8 d ("pre-incubation"). The pre-incubation period served the twofold purpose of: (1) measuring reference O_2 and DIN fluxes to assess the later variation induced by the aggregates; and (2) allowing the establishment of steady-state 15 and 14-DIN gradients in the sediment after the 15N enrichment of the overlying water NO_3^- pool. Water samples were withdrawn from sampling ports positioned at the inlet (three-way valve) and outlet (passive trap) of each chamber (Fig. 1). Exetainers (5.9 mL) were filled for dissolved N_2 analysis and fixed with 100 μL $ZnCl_2$ (50 : 50 vol : vol). Two-milliliter tubes were filled for NO_x^-, NO_2^-, and NH_4^+ analysis and immediately frozen at −20°C. At the end of the "pre-incubation" period, one chamber was opened, 11 aggregates were extracted from the aggregate-production bottles (as described above), and carefully placed onto the sediment surface (density: 1 aggregate × 2 cm^{-2}, total aggregates volume: 241 mm^3). The chamber was then re-sealed and the flow-through incubation was resumed. Water sampling started 5 h after the chamber was sealed and continued in both chambers over the following 7 d (174 h).

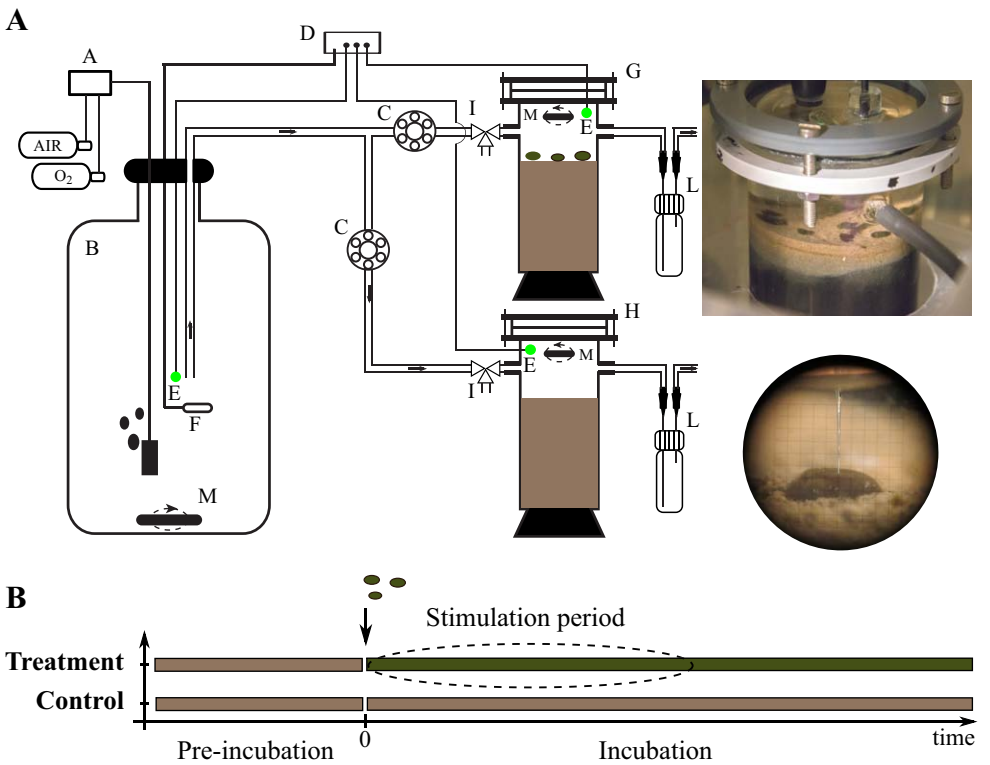

Fig. 1. Panel **A**: The flow-through system used for aggregate incubations. A: gas mixer; B: seawater reservoir; C: peristaltic pumps; D: optic oxygen reader; E: optode spots; F: thermometer; G: treatment chamber with sediment and aggregates; H: control chamber with sediment only; I: three-way valve for inlet sampling; L: passive trap for outlet sampling; M: stirring bar. Top picture: Incubation chamber with aggregates settled on the sediment surface (chamber shaft external diameter: 5.8 cm). Bottom picture: Oxygen microprofile measurement through an aggregate (4.5 mm wide) on the sediment surface. Panel **B**: Diagram of the experimental design. Measurements of O_2 and N dynamics were taken in the treatment and control chambers before (Pre-incubation) and after (Incubation) 11 aggregates were added to the treatment chamber. The brown color indicates that only sediment was present in the chambers; green indicates the presence of aggregates onto the sediment. The arrow indicate the time of aggregates addition. The period named "stimulation" indicates the time interval when the addition of the aggregates substantially altered the benthic O_2 and N dynamics (see text).

Flow-through incubation II – ^{15}N-labeled aggregates

In a separate experiment, we aimed to study the contribution of the aggregates' biomass-bound N to benthic N cycling. ^{15}N-labeled diatoms for aggregate production were thus grown for 3–4 weeks in modified F/2 medium where the original nitrogen source was replaced with a solution of $Na^{14}NO_3$ and $Na^{15}NO_3$ (98 atom% 15N; Sigma-Aldrich) (30 : 70 w : w). After a sediment pre-incubation of 5 d in a flow-through system with seawater amended with 35 μM of unlabeled $^{14}NO_3^-$, the ^{15}N-labeled aggregates were added to one of the two sediment cores at the same density as in the previous experiment. The chamber was then re-sealed and the water flow resumed. The total incubation time was 17 d (380 h), with samplings once or twice per day as described above.

Rate calculation

Oxygen, N_2, and DIN net fluxes between the sediment compartment (sediment or sediment + aggregates) and the overlying water were calculated as:

$$J = (C_o - C_i)\,\frac{V}{A} \quad (1)$$

where J is the net flux, C_o and C_i are the concentrations in the water at the outlet and inlet of the chamber, respectively; V is the water flow rate, and A is the surface area of the sediment core.

Average fluxes ($J_{av.}$) during the pre-incubation and incubation periods were calculated from a finite-interval approximation of the integral of the fluxes measured over the respective time periods:

$$J_{av.} = \frac{1}{b-a}\int_a^b J(t)\;dt \quad (2)$$

where b and a indicate the end and the start time of each period.

Gross NO_3^- fluxes from the benthic compartment to the overlying water (release) was calculated by the changes in concentration and isotopic composition of the NO_3^- pool between the inlet and outlet of each chamber according to Nishio et al. (1983):

$$NO_3^- \text{ release} = \frac{C_i(\text{atom\%}_{out} - \text{atom\%}_{in})}{0.366 - \text{atom\%}_{out}} \times \frac{V}{A} \quad (3)$$

where C_i is the concentration of NO_3^- at the inlet; $\text{atom\%}_{out}$ and $\text{atom\%}_{in}$ are the ^{15}N atom percent of NO_3^- (i.e., $^{15}NO_3^-$: total NO_3^- x 100) at the outlet and inlet, respectively; and *0.366* is the natural abundance of ^{15}N in air (in %). The gross NO_3^- flux from the overlying water to the benthic compartment (uptake) was calculated as the difference between the gross NO_3^- release and the net NO_3^- flux.

Denitrification rates of unlabeled (D_{14}) and ^{15}N-labeled NO_3^- (D_{15}) were calculated from the measured $^{29}N_2$ and $^{30}N_2$ production rates assuming random isotope pairing in the absence of anammox according to Nielsen (1992). Total denitrification rate (D_{tot}) was calculated as the sum of D_{14} and D_{15}. Denitrification sustained by NO_3^- from the water (D_w) was calculated as:

$$D_w = \frac{D_{15}}{\text{atom\%}_{out}} \quad (4)$$

Denitrification coupled to nitrification (D_n) was calculated as the difference between D_{tot} and D_w.

Anammox was quantified on the top 2 cm of sediment via anoxic slurries (2 mL sediment + 8 mL seawater + 2 mL He-headspace in Exetainers), after amended with $^{15}NH_4^+$ and $^{14}NO_3^-$ at 100 μM. Anammox was determined based on the production of $^{29}N_2$ and $^{30}N_2$ divided by the measured fraction of 15N in the NH_4^+ pool. Dinitrogen production via anammox was ratioed to the N_2 production from denitrification determined in parallel incubations with $^{14}NH_4^+$ and $^{15}NO_3^-$. Anammox contributed to the 4% of the total N_2 production and thus was considered negligible for the IPT calculations.

The isotope ratio of ^{15}N-labeled biomass of the aggregates ($R_{agg} = {}^{15}N : {}^{14}N$) was calculated as:

$$R_{agg} = \left(\frac{\delta^{15}N_{agg}}{1000} + 1\right) 0.00366 \quad (5)$$

where $\delta^{15}N_{agg}$ is the isotopic composition of the aggregates biomass with respect to N and 0.00366 (as a fraction of 1) is the natural abundance of ^{15}N in air. Release rates of DIN species from aggregate biomass were estimated from net fluxes of ^{15}N-labeled DIN species calculated according to Eq. 1. However, as the final ^{15}N-labeling percentage of the aggregate biomass was only 60%, the total release of DIN species from aggregate biomass was corrected dividing the flux of ^{15}N-labeled DIN by 0.6.

Chemical analysis

Nitrate and nitrite concentrations were determined on a chemiluminescence detector (CLD 66s, Eco Physics) after being reduced to NO by the VCl_3 (Braman and Hendrix 1989) and NaI (Yang et al. 1997), respectively. Ammonium concentration was measured with the salicylate method (Bower and HolmHansen 1980). The ^{15}N-labeled N_2 was analyzed in the headspace of 5.9 mL Exetainers (Labco, UK) on a gas chromatography-isotopic ratio mass spectrometer (GC-IRMS; Thermo Delta V Plus, Thermo Scientific) (Dalsgaard et al. 2012) with the excess above natural abundance calculated according to Nielsen (1992). ^{15}N-labeled NO_3^-, NO_2^-, and NH_4^+ were analyzed after being converted to N_2 via the cadmium/sulfamic acid, sulfamic acid, and hypobromite assay, respectively (Warembourg 1993; McIlvin and Altabet 2005; Fussel et al. 2012). The resulting ^{15}N-N_2 was analyzed on the GC-IRMS.

Nitrogen isotopic composition ($\delta^{15}N$) and C : N ratio (mol : mol) of the aggregate biomass used for flow-through incubation II (i.e., labeled-aggregates experiment) were determined at the start of the incubation period. To remove ^{14}N and ^{15}N dissolved in the seawater that would otherwise mask the true $\delta^{15}N$ of the biomass, aggregates were washed as follows: approximately 0.5 mL of aggregates ($n = 20$–30) were collected from the aggregate-production bottles and transferred into 15 mL centrifuge tubes filled with 5 mL of NaCl solution (30‰). The tubes were then shaken to resuspend the biomass and gently centrifuged (3000 rpm, 5 min). The supernatant was successively removed and replaced with new NaCl solution. This washing procedure was repeated three times. Samples were then frozen for later analysis. Prior to analysis, samples were thawed and mixed. Small aliquots (150 μL) of dense biomass solution were let dry in aluminum capsules and analyzed on an elemental analyzer coupled to an isotope ratio mass spectrometer (EA-IRMS, Thermo Delta V, Thermo Scientific).

Statistical analysis

The impact of the settlement of aggregates on the benthic processes (fluxes) was assessed by calculating the difference between the fluxes measured in the treatment chamber and control chamber at each time point. A significant change of this difference from the pre-incubation to the stimulation phase was used as evidence of the impact of the aggregates (Underwood 1993). The difference between the two series was assessed by a *t*-test assuming unequal variance.

Results

Aggregate and sediment characterization

The sediment showed a distinct lamination with a top brown/orange layer, an intermediate gray horizon and a deeper (> 1 cm) black layer (Fig. 1). In the top 2 cm, sediment porosity ranged between 0.73 and 0.66, whereas the organic content (LOI) ranged between 2.1% and 3.1% of dry weight (Table 1). Both parameters showed no distinct vertical gradient. The applied aggregates appeared ellipsoidal, compact, and exhibited the golden-brown color (Fig. 1) characteristic of the photopigment fucoxanthin abundantly found in diatoms. The average diameter and volume of the

Table 1. Characteristics of sediment and fresh aggregates (3- to 5-day-old) used in the experiments. Values are reported as Mean (Standard deviation, number of samples). Asterisks (*) indicate that the number refers to the amount of aggregates pooled to run the analysis, and it cannot therefore be interpreted as number of replicates.

Sediment		
Depth interval (mm)	Porosity (v/v)	LOI (dry weight %)
0–5	0.73 (0.005, $n = 3$)	3.1 (0.074, $n = 3$)
5–10	0.66 (0.005, $n = 3$)	2.1 (0.003, $n = 3$)
10–20	0.70 (0.002, $n = 3$)	2.9 (0.084, $n = 3$)
O_2 pen. depth (mm)	4.8 (0.17, $n = 3$)	
O_2 cons. rate (mmol m^{-2} h^{-1})	0.92	
Aggregates		
Max diam. (mm)		3.0 (1.10, n = 67)
Min diam. (mm)		1.3 (0.44, $n = 67$)
Surface area (cm^2)		0.18 (0.14, $n = 67$)
Volume (mm^3)		6.9 (9.4, $n = 67$)
Dry weight (mg mm^{-3})		0.224 ($n = 30$*)
LOI (dry weight %)		48 ($n = 30$*)
C : N		8.7
$ICNO_3^-$ (nmol mm^{-3})		0.93 (0.35, $n = 12$)

aggregates was 2.3 mm (1.2 SD) and 6.9 mm^2 (9.4), respectively. Organic content (LOI) accounted for the 48% of the dry weight (Table 1). The total amount of particulate organic carbon POC and PON delivered to the sediment as aggregate deposition was 6.2 mg and 0.8 mg, respectively.

Oxygen micro-distribution and dynamics on single aggregates

Before the addition of the aggregates, O_2 penetrated on average 4.8 mm into the sediment (O_2 conc. < 1 μM) (Table 1; Fig. 2a,b). The positioning of diatom-aggregates onto the sediment surface remarkably modified the benthic O_2 distribution. Shortly after their settlement, anoxia was detected in the aggregates core (e.g., Fig. 2a,b). The onset of anoxic conditions in the aggregate core varied between 0 and 75 h across all investigated aggregates (six). The anoxic zone of the sediment rose below the aggregates and, in some cases, temporarily merged with the anoxic core of the aggregate (e.g., Fig. 2b). Anoxic conditions were detected either inside or immediately below the aggregate for at least 53 h before the O_2 distribution gradually reverted. Similar dynamics were observed with the same type of aggregates produced on different occasions and placed onto sediment with a shallower O_2 penetration depth (e.g., Fig. 2c).

The reconstructed 2D O_2 distribution from three transect measurements showed a relatively regular O_2 layering before the aggregate settlement (Fig. 2d, Day 0). On day four (Fig. 2d, 76 h), the anoxic zone of the sediment was lifted below the settled aggregate (same specimen analyzed in Fig. 2b). The influence of the aggregate extended beyond the area immediately underneath the aggregate. At 3 mm and 4 mm distance from the aggregate center (coordinate 0 and 1 on the x-axes), the sediment anoxic horizon was lifted 0.3 mm and 0.2 mm, respectively, as compared to the pre-aggregate conditions (i.e., Fig. 2d, Day 0). According to the microprofiles reported in Fig. 2b, the period of maximum expansion of the anoxic zone (30 h) and the development of a separate anoxic microniche (99 h) was missed by this procedure. After 8 d, O_2 penetrated deeper into the aggregate (Fig. 2c, 168 h), and the anoxic area of the sediment had retreated. However, the zone of O_2 depletion remained substantially expanded as compared to the pre-aggregate conditions. For instance, the O_2 concentration at the depth of 1.5 mm below the aggregate center (coordinates $y = 0$, $x = 4$), was only 33 μM as compared to 87 μM prior to aggregate settlement.

Flow-through incubation I: ^{15}N-labeled water

Oxygen and DIN sediment-water exchange

Figure 3 shows net fluxes of O_2, NH_4^+, NO_3^-, and NO_2^- across the sediment-water interface (SWI) in the aggregate and control chambers over a 300-h period. As the fluxes were calculated from the difference in concentration at the outlet and inlet of the chambers, they represent the integrated effect of 11 aggregates on the benthic N transformations and O_2 consumption. The addition of aggregates resulted in an instantaneous increase by 42% of the benthic O_2 uptake. During the 119 h following the aggregates addition (hereafter named "stimulation period"), O_2 uptake decreased gradually to finally re-align with pre-aggregate conditions after 124 h (< 8% change). During the stimulation period, the increased difference between the treatment and control chambers, as compared to the pre-incubation, indicated a significant effect of the addition of aggregates on the benthic O_2 consumption ($p < 0.01$).

Over the stimulation period, the average O_2 consumption in the aggregates chamber increased from 0.92 mmol m^{-2} h^{-1} to 1.1 mmol m^{-2} h^{-1}, resulting in a net additional consumption of 43.7 μmoles of O_2. Assuming a respiratory quotient (oxygen : carbon) of 1, such increase in O_2 consumption would have corresponded to the mineralization of 8% of the total aggregate-associated POC.

In the flow-through chamber, the aggregates covered 1.7 cm^2 of sediment (equal to 8.7% of the total sediment surface). The estimated volume of the anoxic cones projected from the base of each aggregate (considering an expansion of the anoxic zone similar to the one measured at 76 h) was 1.1 cm^3, which corresponds to approximately 11% of the initial oxic volume of the sediment core.

Following the addition of aggregates, the sediment transiently turned into a net source of NH_4^+. However, after 47 h, the flux returned to negative values, indicating net uptake (Fig. 3a). On average, NH_4^+ net uptake in the

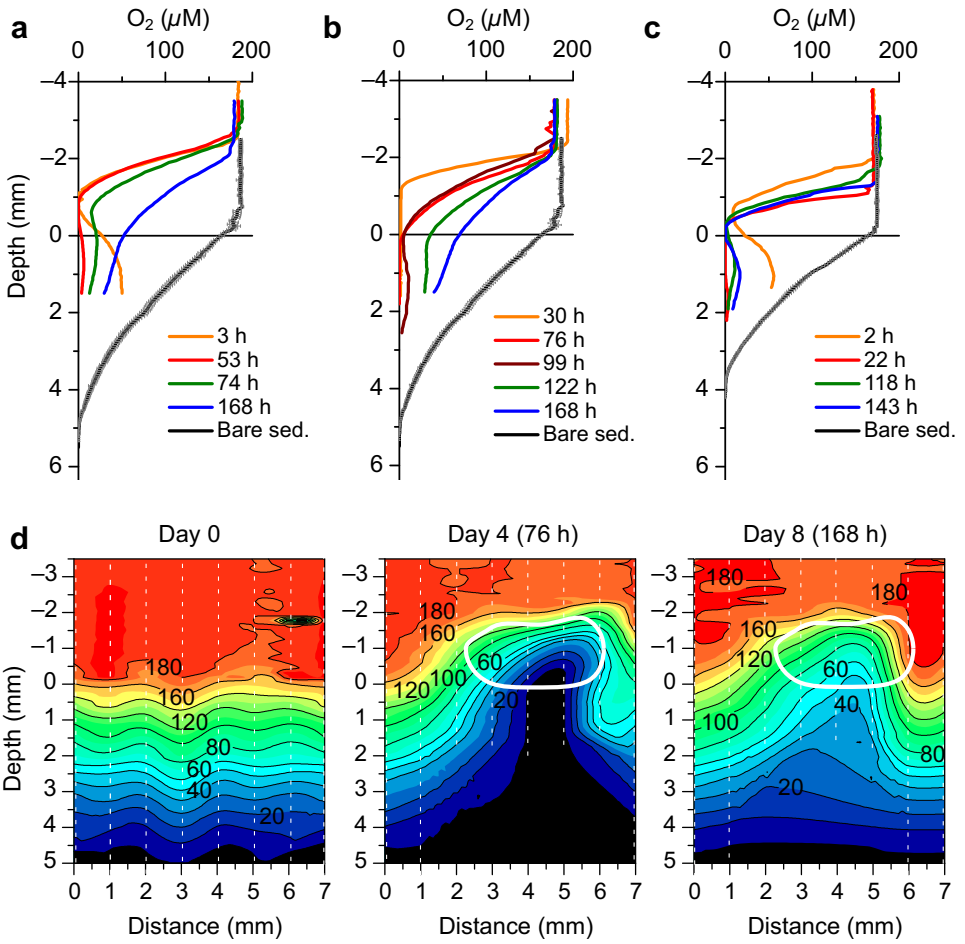

Fig. 2. (**a**, **b**) Oxygen microprofiles measured through the center of two different aggregates positioned on the sediment surface (aggregates and sediment were of the same type as the ones used for the flow-through incubations). Black lines indicate microprofiles (mean ± SEM, $n = 3$) measured in the sediment before the addition of the aggregates (bare sediment). The zero value on the *y*-axes indicates the sediment–water interface (the aggregate surface is at approx. −1.8 mm). (**c**) Oxygen microprofiles measured through the center of an aggregate positioned on a sediment with a shallower O_2 penetration depth. (**d**) Variation of the O_2 microdistribution at the sediment–water interface before and after (two time points) the settlement of the aggregate profiled in Fig. 2b. The 2D oxygen microdistribution in each picture has been reconstructed by the interpolation of vertical microprofiles (dotted lines) measured across the longer horizontal axis of the aggregate. Aggregate approximate position and shape is outlined by the white line. Zero on the *y*-axes corresponds to the sediment surface. Numbers on isopleths indicate O_2 concentration (μM).

aggregate chamber decreased from 4.0 μmol m^{-2} h^{-1} during the pre-incubation period to 2.4 μmol m^{-2} h^{-1} during the stimulation period. The analysis of the difference between the two chambers revealed a significant effect of the aggregates during the stimulation period ($p = 0.04$). Net $^{15}NH_4^+$ production was measured throughout the experiment, indicating ongoing DNRA activity. During the stimulation period, the net production of $^{15}NH_4^+$ decreased from 3.2 (pre-incubation) to 2.1 μmol m^{-2} h^{-1} (data not shown).

The average NO_2^- production increased from zero to 1.1 μmol m^{-2} h^{-1} during the first 69 h of incubation, before conditions reverted to no net exchange (Fig. 3b). At 5, 45, and 53 h, $^{15}NO_2^-$ accounted for 71%, 59%, and 82% of the total net NO_2^- production, respectively, indicating reduction of NO_3^- from the overlying water as the main source of NO_2^-. No significant changes (< 0.04 μmol m^{-2} h^{-1}) in the average NO_2^- fluxes were measured in the control chamber.

Within the stimulation period, net NO_3^- uptake peaked in two main events (21 and 98 h) (Fig. 3b). The average net NO_3^- uptake increased from 26.9 (pre-incubation) to 30.5 μmol m^{-2} h^{-1}. During the same period, the average NO_3^- uptake in the control chamber varied from 25.7 μmol m^{-2} h^{-1} to 21.3 μmol m^{-2} h^{-1}, but without any clear temporal trend. For the whole 119 h stimulation period, the difference between the two chambers was not significant ($p = 0.09$), whereas it was significant for the first 98 h ($p = 0.04$). During the stimulation period, the NO_3^- pool in the aggregate chamber became depleted in ^{15}N, i.e., the ^{15}N atom fraction of NO_3^- decreased from 0.87 ± 0.04 (Mean ± SD, $n = 5$) during the pre-incubation to 0.77 ± 0.07 ($n = 10$) during the

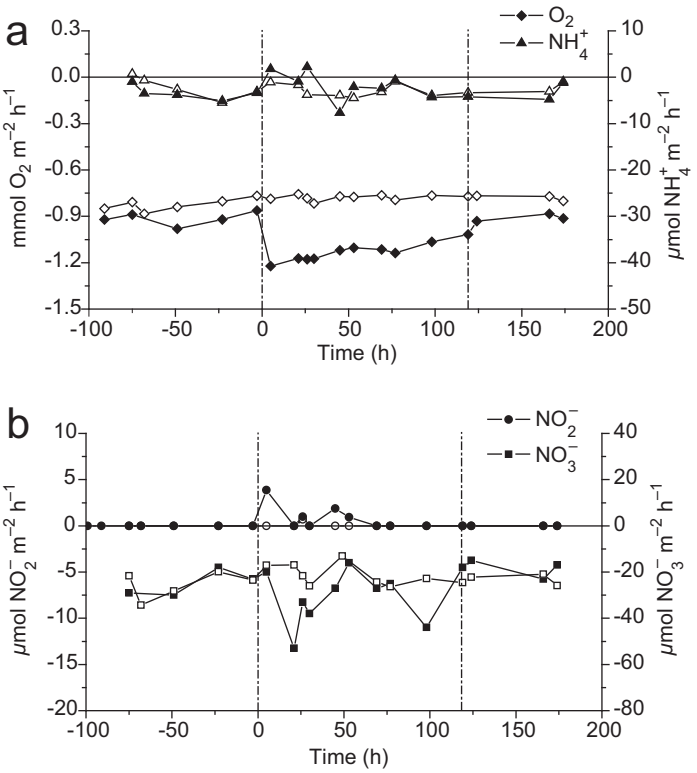

Fig. 3. Time series of O_2 and NH_4^+ (**a**), and NO_3^- and NO_2^- (**b**) net fluxes across the sediment–water interface, in the aggregate (full symbols) and control (empty symbols) chambers. The zero on the *x*-axes indicates the time when aggregates were placed onto the sediment surface. The two dotted lines remark the start and the end of the 119 h period of enhanced O_2 consumption (stimulation period).

incubation period. Conversely, the value remained constant in the control chamber, i.e., 0.85 ± 0.03 ($n = 5$) and 0.85 ± 0.09 ($n = 13$) during the pre-incubation and incubation, respectively. The decrease in the difference between the ^{15}N atom fraction in the control and aggregate chamber after the addition of the aggregates was significant ($p = 0.03$).

Estimation of the gross NO_3^- fluxes indicated that both gross NO_3^- uptake and release were stimulated by the addition of aggregates. Within the stimulation period, the gross NO_3^- uptake increased from -37.4 µmol m^{-2} h^{-1} to -49.4 µmol m^{-2} h^{-1} (Fig. 6), whereas the gross NO_3^- release increased from 10.5 µmol m^{-2} h^{-1} to 18.9 µmol m^{-2} h^{-1}. The $ICNO_3$ pool estimated at the incubation start and end was 184 nmol and 9.3 nmol, respectively.

The release of intracellularly stored NO_3^- by diatoms throughout the incubation (174 h), was thus 175 nmol, corresponding to an average flux of 0.7 µmol NO_3^- m^{-2} h^{-1} during the stimulation period (Fig. 6).

Dynamics of total denitrification and of its components D_w *and* D_n

Control and aggregates chambers showed constant $^{29}N_2$ and $^{30}N_2$ fluxes during the pre-incubation indicating steady-state conditions (Fig. 4a). The differences between the two chambers denoted a natural heterogeneity between the intact sediment cores. The addition of the aggregates stimulated both fluxes. On average, during the stimulation period, $^{29}N_2$ and $^{30}N_2$ fluxes increased by the 36% and 211%, respectively. The increase was largely reabsorbed after the

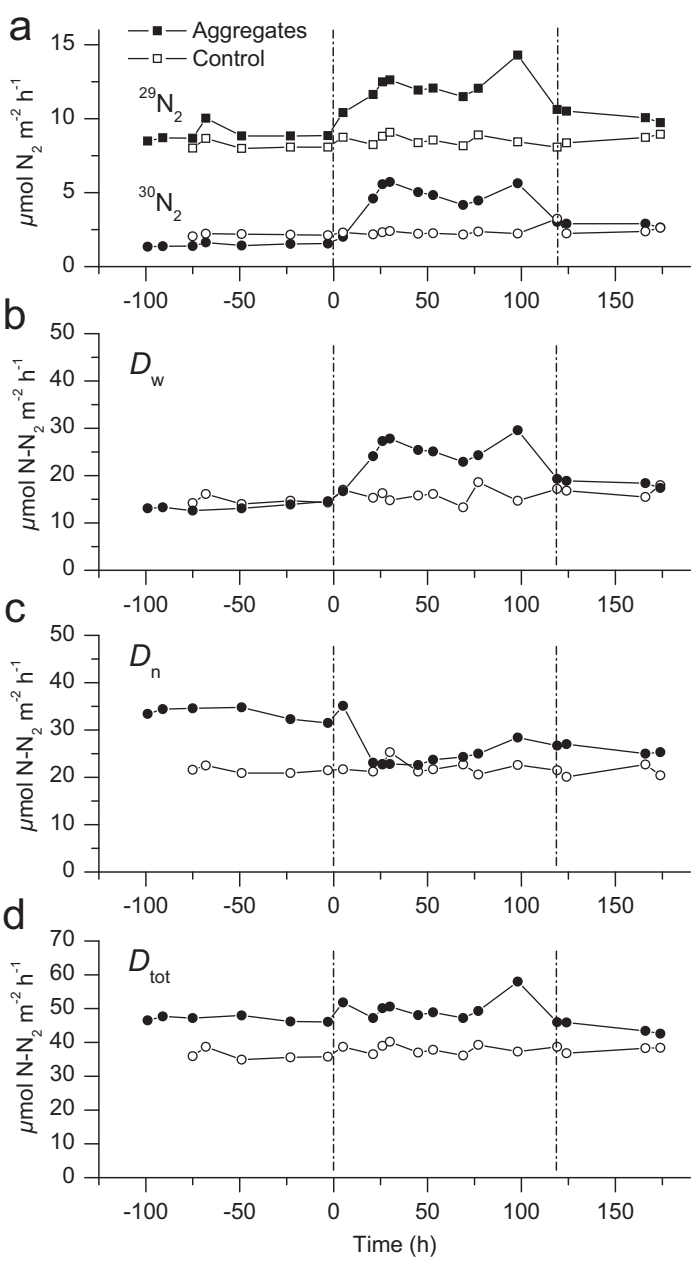

Fig. 4. Time series of: (**a**) $29N_2$ and $30N_2$ production rates; (**b**) denitrification sustained by NO_3^- from the water column (D_w); (**c**) denitrification sustained by NO_3^- from nitrification (D_n); and (**d**) total denitrification rate (D_{tot}). Full and empty circles indicate rates measured in the aggregate and control chambers, respectively. The zero on the *x*-axes indicates the time when aggregates were placed onto the sediment surface. The two dotted lines remark the start and the end of the 119 h period of enhanced O_2 consumption (stimulation period).

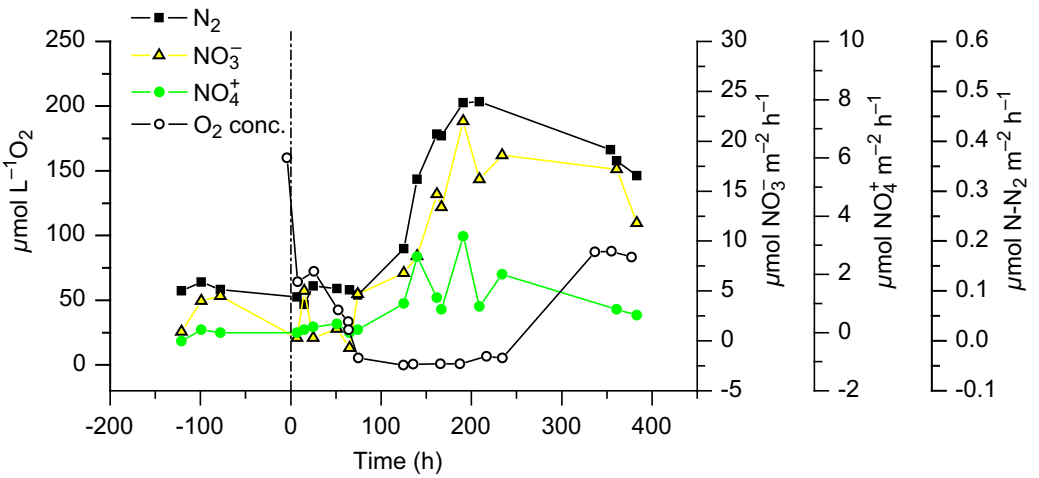

Fig. 5. Net NO_3^-, NH_4^+, and N-N_2 release rates from aggregate biomass-bound nitrogen throughout the pre-incubation and incubation period in the aggregate chamber. Nitrate, NH_4^+, and N-N_2 release rates were calculated from $^{15}NO_3^-$, $^{15}NH_4^+$, and $^{29}N_2$ rates, respectively, corrected for the labeling fraction of the aggregate biomass (≈ 60%). Empty circles indicate O_2 concentration measured at the center of an aggregate (via O_2 microsensor) in a parallel incubation.

stimulation period, when on average, $^{29}N_2$ and $^{30}N_2$ fluxes remained only 15% and 96% higher as compared to the pre-incubation level, respectively.

In accordance with the observed increase in gross NO_3^- uptake, the addition of aggregates stimulated denitrification fueled by NO_3^- from the overlying water (D_w) (Fig. 4b). The increase in D_w in the aggregates chamber as compared to the control chamber was significant ($p < 0.01$). The average D_w within the stimulation period was 80% higher (+10.8 µmol m^{-2} h^{-1}) than during the pre-incubation (13.5 µmol N m^{-2} h^{-1}) (Fig. 6). Between 119 and 174 h, the average D_w decreased to 17.5 µmol N m^{-2} h^{-1}, thus still remaining 29% higher than during the pre-incubation period. In contrast, the fraction of denitrification fueled by nitrification (D_n) decreased from the average pre-incubation level of 33.4 to 22.8 µmol N m^{-2} h^{-1} at 21 h (Fig. 4c). Later measurements (21–174 h) indicate a slow but significant increase in the rate of D_n with time ($D_n = 22.7 + 0.024 \times$ hour; $t(11) = 2.76$, $p = 0.02$). At the end of the incubation (174 h), D_n was still 24% lower than during the pre-incubation period (25.3 µmol N m^{-2} h^{-1}). The average D_n within the stimulation period was 26.0 µmol N m^{-2} h^{-1} (Fig. 6). The drop of D_n in the aggregates chamber as compared to the control chamber during the stimulation period was significant ($p < 0.01$).

The opposing effects on D_w and D_n resulted in a non-significant ($p = 0.40$) change in the total denitrification rate (D_{tot}) during the stimulation period (Fig. 4d). Within the first 76 h, the difference in D_{tot} between aggregate and control chamber (11.1 ± 0.5 µmol N m^{-2} h^{-1}, M ± SD, $n = 8$) did not change as compared to the one recorded during the pre-incubation (11.3 ± 1.2 µmol N m^{-2} h^{-1}, $n = 4$). At 98 h, however, the difference transiently increased to 20.8 µmol N m^{-2} h^{-1} (+83%). Later measurements realigned to the pre-incubation level. In the aggregate chamber, the average D_{tot} in the pre-incubation and stimulation period was 47.1 µmol N m^{-2} h^{-1} and 50.3 µmol N m^{-2} h^{-1}, respectively (Fig. 6). No major variation in D_{tot}, D_w, and D_n were recorded in the control chamber between the pre-incubation and the incubation period.

Flow-through incubation II: ^{15}N-labeled aggregate biomass

To evaluate the importance of aggregate-associated N for the overall benthic N cycling upon aggregate settlement, ^{15}N-labeled aggregates were added to the sediment in the flow-through chamber in a separate experiment. Here, labeled DIN was released into the overlying water following the addition of aggregates onto the sediment surface (Fig. 5). The efflux of ^{15}N-labeled N_2, NO_3^-, and NH_4^+ began after 74 h, and coincided with the onset of anoxia at the core of the aggregate. ^{15}N fluxes peaked at approx. 200 h, and then gradually decreased until the end of the incubation. By the last sampling time point (383 h), the fluxes of N_2, NO_3^-, and NH_4^+ had decreased to 60%, 46%, and 20% of their maximum increases, respectively.

Between 74 and 383 h, the average fluxes of N_2-N, NH_4^+, and NO_3^- derived from mineralization of aggregate biomass corresponded to 0.2 µmol N m^{-2} h^{-1}, 1.2 µmol N m^{-2} h^{-1}, and 10.1 µmol N m^{-2} h^{-1}, respectively (Fig. 6). Within the same time-interval, such fluxes released 0.16 µmol, 0.84 µmol, and 7.1 µmol of N_2-N, NH_4^+, and NO_3^-, respectively. The release of $ICNO_3$ only accounted for 1.5% of the net NO_3^- release into the overlying water. The sum of the inorganic N emission accounted for the mineralization of the 13.7% of the aggregates' biomass-bound N pool. No net release of ^{15}N-labeled inorganic nitrogen species nor

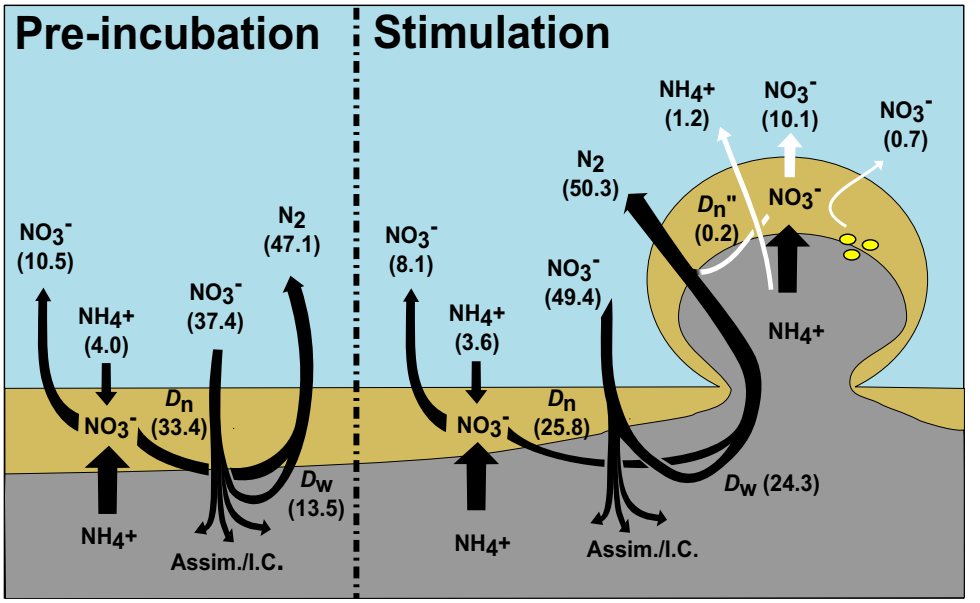

Fig. 6. Fluxes across the sediment–water and aggregate–water interfaces of DIN species during the pre-incubation (sediment only) and stimulation periods (sediment + aggregates). Gray and beige areas represent anoxic and oxic zones of the sediment, respectively. Yellow circles symbolize diatoms cells. Fluxes are reported as averages over 75 h for the pre-incubation period and 119 h for the stimulation period. All values are in μmol N m^{-2} h^{-1}. Fluxes representative of the total exchange between water and sediment + aggregates were calculate from experiment 1. Fluxes of D_w and D_n were estimated via the Isotope Pairing Technique; NO_3^- fluxes indicate gross fluxes calculated via Eq. 3, and NH_4^+ fluxes indicate net fluxes calculated via Eq. 2. For the stimulation period, the contribution of mineralized aggregates biomass to the NO_3^-, NH_4^+, and N_2 fluxes (as estimated from experiment II with labeled aggregates) is indicated by white arrows. To avoid double counting, the mere contribution of the sediment has been calculated by subtracting NO_3^-, NH_4^+, and N_2 fluxes from the aggregates biomass from the gross NO_3^- release (18.9), net NH_4^+ uptake (–2.4), and D_n (26.0), respectively, as calculated from experiment I (*see* "Result" section).

significant increase in the O_2 consumption rate were measured in the control incubation (data not shown).

Discussion

Aggregate effect on benthic O_2 consumption and distribution

Settled diatom-aggregates remarkably modified the O_2 distribution in the sediment and enhanced the benthic O_2 demand. Hypoxic/anoxic areas developed inside the aggregates within a few hours from their settlement, indicating high mineralization activity and limited diffusive O_2 transport (Ploug et al. 1997). Anoxic zones were persistently measured within or immediately below the aggregates for up to 53–143 h. Temporary (7–8 h) anoxic niches have been reported, by applying planar optodes, at the center of 2 mm diatom-aggregates produced similarly to the ones used in this study and settled on marine sediment overlain with air-saturated water (Glud 2008; Lehto et al. 2014). This is much shorter than the lifetime of aggregate-associated anoxia observed in our experiments, and it might be due to the lower O_2 level of the overlying water in our incubations. Noticeably, however, our measurements have to be considered conservative as, contrary to planar optodes that limit O_2 transport through the plane of measurements (Santner et al. 2015), microsensor application can enhance the transport of O_2 into the aggregates by both compressing the diffusive boundary layer (Glud et al. 1994) and physically piercing the aggregate.

Our transect measurements showed how the aggregates can influence the benthic O_2 distribution beyond the area that they physically occupy inducing changes at up to $\sim$ 5 mm distance into the sediment. The sediment anoxic horizon consistently rose beneath the aggregates in all incubations. Time-series measurements indicated that this state persisted even once oxic/hypoxic conditions had re-established inside the aggregates. The expansion of the anoxic and zone of the sediment is likely the result of the O_2 supply limitation due to both the active O_2 consumption occurring within the aggregates and the longer diffusion pathway imposed by their physical presence. Dissolved organic carbon (DOC) and inorganic nutrient released from sinking aggregates have been shown to enhance microbial activity in pelagic systems (Kiorboe 2001; Azam and Malfatti 2007; Stocker et al. 2008). Likewise, the release of DIN and labile DOC from the settled aggregates (that have 15 times higher concentration of, and most likely also more reactive, OM than the sediment) could have enhanced the metabolic activity of the heterotrophic microbial community in the sediment underneath the aggregates.

Aggregate effect on DIN fluxes at the sediment–water interface

The settlement of aggregates transiently enhanced both the gross release and uptake of NO_3^- (which together resulted in an enhanced net NO_3^- consumption), and stimulated the net production of NO_2^- and NH_4^+ of the benthic compartment. The average increase in gross NO_3^- uptake accounted for the 91% of the increase in D_w (Fig. 6), suggesting that the increased denitrification activity drove the enhanced benthic NO_3^- consumption (see later discussion). The increased gross NO_3^- release indicated an input of $^{14}NO_3^-$. Possible sources of $^{14}NO_3^-$ are nitrification activity in the sediment or in the aggregates, and $ICNO_3$ release from the aggregate-associated diatoms. Intracellular NO_3^- concentrations in our aggregates (Table 1) aligned with previous studies on *S. marinoi* aggregates (Stief et al. 2016). The almost complete release (98%) of the $ICNO_3$ pool during the incubation experiment can however only account for 8.9% of the increase in gross NO_3^- release. Instead, the gross release of NO_3^- was more likely derived from degrading aggregate biomass as indicated by the following ^{15}N-labeled aggregates experiment. Accordingly, the average rate of NO_3^- release from the ^{15}N-labeled aggregates was very similar to the average increase in gross NO_3^- release measured in the experiment with $^{15}NO_3^-$ labeled water (8.4 μmol m^{-2} h^{-1}). As ^{15}N in the labeled aggregates was almost exclusively (99.8%) present as organic N, the increase in gross NO_3^- release has to be attributed to nitrification activity fueled by NH_4^+ liberated during mineralization of the aggregate biomass.

In contrast to O_2 consumption, that was substantially elevated throughout the whole stimulation period, net NO_3^- consumption peaked in two main events. Net NO_3^- consumption summarizes gross NO_3^- uptake and gross NO_3^- release, which in turn respond to the expansion of the anoxic zone (and the consequent increase in D_w) and to the increase nitrification activity at the aggregate surface, respectively. These two events do not necessarily occur simultaneously. Their asynchronous occurrence is likely causing the intermittent increase in net NO_3^- consumption.

The sediment was generally a net sink for NH_4^+, which is consistent with nitrification activity in the surface layer (Stief et al. 2003). However, following the addition of aggregates, the average sediment net NH_4^+ uptake decreased and sporadic net NH_4^+ effluxes were recorded. Of the reduced net NH_4^+ uptake during the stimulation period, 75% can be attributed to enhanced NH_4^+ release from mineralization of aggregate biomass as calculated from the experiment with ^{15}N-labeled aggregates. Potentially, the stimulation of dissimilatory nitrate reduction to ammonium (DNRA) could also have contributed to the reduced net NH_4^+ uptake. This possibility was, however discarded, as the production of $^{15}NH_4^+$ did not increase throughout the experiment with $^{15}NO_3^-$ enriched water. The residual 25% of the decrease in net NH_4^+ uptake has thus to be attributed to a decreased sediment nitrification efficiency, which was also suggested by the concurrent drop in D_n.

Net NO_2^- production was recorded during the initial phase of the incubation. Between the 59% and 82% of such emission was sustained by $^{15}NO_2^-$ production. Considering that the only source of ^{15}N was NO_3^- dissolved in the overlying water, and the ^{15}N atom percentage of NO_3^- at the inlet (i.e., 86%), such $^{15}NO_2^-$ production rates indicates that 68–96% of the total net NO_2^- production can be attributed to incomplete denitrification of overlying water NO_3^-.

Aggregate effect on benthic denitrification and nitrification

The addition of the aggregates substantially stimulated $^{29}N_2$ and $^{30}N_2$ production. The period of maximum production aligned with the stimulation period further suggesting that the reduced O_2 availability stimulated denitrification. The residual stimulation of the production rates persisting during later measurements was likely due to a longer, less acute effect of the aggregates settlement (e.g., slow mineralization of recalcitrant OM). The settlement of aggregates increased the rate of denitrification fueled by NO_3^- from the overlying water (D_w) and decreased the contribution of denitrification fueled by NO_3^- from sedimentary nitrification (D_n). The net effect on the total denitrification (D_{tot}), however, was negligible during most of the incubation period. Only when D_n recovered some time after the aggregate deposition, the D_{tot} increased substantially. The stimulation of D_w was probably favored by the expansion and branching of the anoxic sediment horizon below and inside the aggregates and the thinning of the oxic surface layer, which together increased the total exchange surface and reduced the diffusion pathway for NO_3^- from the overlying water. The inverse relationship between O_2 penetration depth and D_w intensity has been shown in previous studies (e.g., Christensen et al. 1990; Rysgaard et al. 1995). The denitrifying community which is generally considered to consist of mainly facultative anaerobes (Zumft 1997), is expected to rapidly switch from O_2 to NO_3^- respiration when O_2 is no longer available. Denitrifiers could further capitalize on the elevated input of labile organic carbon released from the decaying aggregates. In addition, the lifting of the anoxic zone could have stimulated other anaerobic metabolisms (i.e., sulfate and iron oxides reduction) increasing the availability of H_2S and Fe^{2+} at shallower depths that could in turn, contributed to increase NO_3^- reduction. However, iron-dependent NO_3^- reduction is expected to primarily produce NH_4^+ (Robertson et al. 2016). Increase in DNRA activity was not recorded after the addition of the aggregates. Therefore, such metabolisms, if active, must have been constrained to a marginal role.

The reduced oxic portion of the sediment diminished the volume suitable for nitrification. It is to expect that upon an abrupt shrinkage of the oxic zone, the integrated nitrifying activity will be suppressed, at least transiently, until the

microorganisms in the remaining oxic zone possibly increase their activity in response to the altered substrate concentrations. Furthermore, the accumulation of H_2S at shallower depth due to the likely lifting of the SO_4^{2-} reduction zone, could have further inhibited nitrification activity (e.g., Joye and Hollibaugh 1995). The slow and gradual recovery of the D_n after the initial inhibition period aligned with the gradual re-oxygenation of the sediment as shown by the microprofiles.

The aggregate-induced change in local O_2 availability is thus likely to cause a suppression of nitrification activity and an immediate stimulation of denitrification activity transiently uncoupling the two processes. High input of OM to intertidal sediment has been previously shown to both stimulate D_w (e.g., Caffrey 1993) and inhibit sediment nitrification (Caffrey 1993; Sloth 1995). However, these observations have been made in experimental set-ups where high loads of OM (12–40 g C m^{-2}) have been homogeneously spread onto the sediment surface, or mixed within the top sediment layer. Our study shows how similar effects may occur with lower loads (3.1 g C m^{-2}), if the OM is delivered to the sediment, unevenly, as concentrated packages such as during the more realistic settlement of algae-aggregates. In sediment with deeper O_2 penetration, such as the one typical of deep-sea environments, the inhibition of the D_n would virtually be marginal (or absent) resulting in a more pronounced increase of the total denitrification. Aggregates burial as possibly induced by benthic fauna would further limit mass-transfer processes around the aggregates. Such circumstances would favor the development of larger or longer lasting anoxic niches, with more pronounced effect on the benthic nitrogen cycling.

Conversely to the decrease in sediment nitrification, NO_3^- was the main N species released by the mineralization (and consequent oxidation) of aggregate biomass (NO_3^- : NH_4^+ : N-N_2 emission = 43 : 5 : 1) indicating pronounced nitrification activity in the oxic part of the aggregates (Fig. 6). Such efficient nitrification activity contrasts with recent reports on sinking aggregates where NH_4^+ release from mineralization was high and nitrification activity was negligible (Klawonn et al. 2015; Ploug and Bergkvist 2015; Stief et al. 2016). The lack of nitrification activity in sinking aggregates has been ascribed to the long doubling time of nitrifiers. On the sediment, inoculation of nitrifiers from the benthic community might have contributed to the establishment of such high rates of nitrification. The high NO_3^- : N-N_2 fluxes ratio indicates a weak coupling between nitrification and denitrification at the aggregate surface and that the newly produced NO_3^- mainly diffused into the overlying water, presumably due to the small anoxic portion of the aggregate and the elliptical geometry of the aging aggregates.

Summary and perspectives

Diatom-aggregates influenced the benthic turn-over of O_2 and nitrogen in several ways. Their settlement enhanced the net benthic O_2 and NO_3^- consumption and concurrently stimulated the NO_2^- and NH_4^+ production. The shift in O_2 availability and diffusional pathways favored the denitrification of NO_3^- from the overlying water at the expense of coupled nitrification-denitrification; this was partly due to a transient suppression of sediment nitrification. Furthermore, stimulated nitrification in the aggregates mainly induced a net release of NO_3^- to the overlying water (Fig. 6). These effects were dynamic and were largely exhausted within 5–20 d.

The study demonstrates that the partitioning of micro-niches induced by the aggregates settlement impacts the benthic N cycling, and it furthermore provides a time-frame for such impacts. Because of their ephemeral nature, these niches have so far been overlooked. Within the span of reported sinking velocities i.e., 10–569 m d^{-1} (e.g., Ploug et al. 1999; Iversen et al. 2010), 3- to 5-day-old aggregate such as the ones used in this study could reach the seafloor at water depths ranging between 10 m and > 2800 m. The scattered deposition of aggregates can therefore contribute to determine the mosaic nature of sediments, and to set the temporal variation (succession from aerobic to anaerobic metabolisms) in confined microbial communities from coastal to deep-sea benthic environments.

Climate-induced increases in phytoplankton productivity might enhance the export of biomass to the sediment in the form of aggregates especially in polar settings. This will potentially increase the microniche structure and, as seen here, affect benthic nitrogen (and possibly other nutrients) cycling.

References

Alldredge, A. L., and Y. Cohen. 1987. Can microscale chemical patches persist in the sea? Microelectrode study of marine snow, fecal pellets. Science **235**: 689–691. doi: 10.1126/science.235.4789.689

Azam, F., and F. Malfatti. 2007. Microbial structuring of marine ecosystems. Nat. Rev. Microbiol. **5**: 782–791. doi: 10.1038/nrmicro1747

Boetius, A., and others. 2013. Export of algal biomass from the melting Arctic Sea ice. Science **339**: 1430–1432. doi: 10.1126/science.1231346

Bower, C. E., and T. HolmHansen. 1980. A salicylate-hypochlorite method for determining ammonia in seawater. Can. J. Fish. Aquat. Sci. **37**: 794–798. doi:10.1139/f80-106

Braman, R. S., and S. A. Hendrix. 1989. Nanogram nitrite and nitrate determination in environmental and biological-materials by vanadium(III) reduction with chemi-luminescence detection. Anal. Chem. **61**: 2715–2718. doi:10.1021/ac00199a007

Caffrey, J. M., N. P. Sloth, H. F. Kaspar, and T. H. Blackburn. 1993. Effect of Organic Loading on Nitrification and

Denitrification in a Marine Sediment Microcosm. Fems Microbiol Ecol **12**: 159–167.

Christensen, P. B., L. P. Nielsen, J. Sorensen, and N. P. Revsbech. 1990. Denitrification in nitrate-rich streams - diurnal and seasonal-variation related to benthic oxygen-metabolism. Limnol. Oceanogr. **35**: 640–651. doi:10.4319/lo.1990.35.3.0640

Dalsgaard, T., B. Thamdrup, L. Farías, and N. P. Revsbech. 2012. Anammox and denitrification in the oxygen minimum zone of the eastern South Pacific. Limnol. Oceanogr. **57**: 1331–1346. doi:10.4319/lo.2012.57.5.1331

Eugster, O., and N. Gruber. 2012. A probabilistic estimate of global marine N-fixation and denitrification. Global Biogeochem. Cycles **26**: 1–15. doi:10.1029/2012GB004300

Fussel, J., P. Lam, G. Lavik, M. M. Jensen, M. Holtappels, M. Gunter, and M. M. M. Kuypers. 2012. Nitrite oxidation in the Namibian oxygen minimum zone. ISME J. **6**: 1200–1209. doi:10.1038/ismej.2011.178

Glud, R. N. 2008. Oxygen dynamics of marine sediments. Mar. Biol. Res. **4**: 243–289. doi:10.1080/17451000801888726

Glud, R. N., J. K. Gundersen, N. P. Revsbech, and B. B. Jorgensen. 1994. Effects on the benthic diffusive boundary-layer imposed by microelectrodes. Limnol. Oceanogr. **39**: 462–467. doi:10.4319/lo.1994.39.2.0462

Glud, R. N., F. Wenzhofer, A. Tengberg, M. Middelboe, K. Oguri, and H. Kitazato. 2005. Distribution of oxygen in surface sediments from central Sagami Bay, Japan: In situ measurements by microelectrodes and planar optodes. Deep-Sea Res. Part I **52**: 1974–1987. doi:10.1016/j.dsr.2005.05.004

Glud, R. N., H. Stahl, P. Berg, F. Wenzhofer, K. Oguri, and H. Kitazato. 2009. In situ microscale variation in distribution and consumption of O-2: A case study from a deep ocean margin sediment (Sagami Bay, Japan). Limnol. Oceanogr. **54**: 1–12. doi:10.4319/lo.2009.54.1.0001

Glud, R. N., S. Rysgaard, G. Turner, D. F. McGinnis, and R. J. G. Leakey. 2014. Biological- and physical-induced oxygen dynamics in melting sea ice of the Fram Strait. Limnol. Oceanogr. **59**: 1097–1111. doi:10.4319/lo.2014.59.4.1097

Guillard, R. R., and J. H. Ryther. 1962. Studies of marine planktonic diatoms. I. Cyclotella nana Hustedt, and Detonula confervacea (cleve) Gran. Can. J. Microbiol. **8**: 229–239. doi:10.1139/m62-029

Iversen, M. H., N. Nowald, H. Ploug, G. A. Jackson, and G. Fischer. 2010. High resolution profiles of vertical particulate organic matter export off Cape Blanc, Mauritania: Degradation processes and ballasting effects. Deep-Sea Res. Part I57: 771–784. doi:10.1016/j.dsr.2010.03.007

Joye, S. B., and J. T. Hollibaugh. 1995. Influence of sulfide inhibition of nitrification on nitrogen regeneration in sediments. Science **270**: 623–625. doi:10.1126/science.270.5236.623

Kamp, A., D. de Beer, J. L. Nitsch, G. Lavik, and P. Stief. 2011. Diatoms respire nitrate to survive dark and anoxic conditions. Proc. Natl. Acad. Sci. USA **108**: 5649–5654. doi:10.1073/pnas.1015744108

Kamp, A., P. Stief, J. Knappe, and D. de Beer. 2013. Response of the ubiquitous pelagic diatom Thalassiosira weissflogii to darkness and anoxia. Plos One **8**. doi:10.1371/journal.pone.0082605

Kamp, A., P. Stief, L. A. Bristow, B. Thamdrup, and R. N. Glud. 2016. Intracellular nitrate of marine diatoms as a driver of anaerobic nitrogen cycling in sinking aggregates. Front. Microbiol. **7**. doi:10.3389/fmicb.2016.01669

Kanneworff, E., and W. Nicolaisen. 1972. The "Haps" a frame-supported bottom corer. Ophelia **10**: 119–128. doi:10.1080/00785326.1972.10430108

Kiorboe, T. 2001. Formation and fate of marine snow: Small-scale processes with large-scale implications. Sci. Mar. **65**: 57–71. doi:10.3989/scimar.2001.65s257

Kiorboe, T., H. P. Grossart, H. Ploug, and K. Tang. 2002. Mechanisms and rates of bacterial colonization of sinking aggregates. Appl. Environ. Microb. **68**: 3996–4006. doi:10.1128/AEM.68.8.3996-4006.2002

Klawonn, I., S. Bonaglia, V. Bruchert, and H. Ploug. 2015. Aerobic and anaerobic nitrogen transformation processes in N-fixing cyanobacterial aggregates. ISME J. **9**: 1456–1466. doi:10.1038/ismej.2014.232.

Lehto, N., R. N. Glud, G. A. Nordi, H. Zhang, and W. Davison. 2014. Anoxic microniches in marine sediments induced by aggregate settlement: Biogeochemical dynamics and implications. Biogeochemistry **119**: 307–327. doi:10.1007/s10533-014-9967-0

Lomas, M. W., and P. M. Glibert. 2000. Comparisons of nitrate uptake, storage, and reduction in marine diatoms and flagellates. J. Phycol. **36**: 903–913. doi:10.1046/j.1529-8817.2000.99029.x

McIlvin, M. R., and M. A. Altabet. 2005. Chemical conversion of nitrate and nitrite to nitrous oxide for nitrogen and oxygen isotopic analysis in freshwater and seawater. Anal. Chem. **77**: 5589–5595. doi:10.1021/ac050528s

Nielsen, L. P. 1992. Denitrification in sediment determined from nitrogen isotope pairing. FEMS Microbiol. Ecol. **86**: 357–362. doi:10.1016/0378-1097(92)90800-4

Nishio, T., I. Koike, and A. Hattori. 1983. Estimates of denitrification and nitrification in coastal and estuarine sediments. Appl. Environ. Microb. **45**: 444–450. doi:0099-2240/83/020444-07$02.00/0

Ploug, H., M. Kuhl, B. BuchholzCleven, and B. B. Jorgensen. 1997. Anoxic aggregates - an ephemeral phenomenon in the pelagic environment? Aquat. Microb. Ecol. **13**: 285–294. doi:10.3354/ame013285

Ploug, H., and H. P. Grossart. 1999. Bacterial production and respiration in suspended aggregates - a matter of the incubation method. Aquat. Microb. Ecol. **20**: 21–29. doi:10.3354/ame020021

Ploug, H., H. P. Grossart, F. Azam, and B. B. Jorgensen. 1999. Photosynthesis, respiration, and carbon turnover in

sinking marine snow from surface waters of Southern California Bight: Implications for the carbon cycle in the ocean. Mar. Ecol. Prog. Ser. **179**: 1–11. doi:10.3354/meps179001

Ploug, H., and H. P. Grossart. 2000. Bacterial growth and grazing on diatom aggregates: Respiratory carbon turnover as a function of aggregate size and sinking velocity. Limnol. Oceanogr. **45**: 1467–1475. doi:10.4319/lo.2000.45.7.1467

Ploug, H., and J. Bergkvist. 2015. Oxygen diffusion limitation and ammonium production within sinking diatom aggregates under hypoxic and anoxic conditions. Mar. Chem. **176**: 142–149. doi:10.1016/j.marchem.2015.08.012

Rabouille, C., L. Denis, K. Dedieu, G. Stora, B. Lansard, and C. Grenz. 2003. Oxygen demand in coastal marine sediments: Comparing in situ microelectrodes and laboratory core incubations. J. Exp. Mar. Biol. Ecol. **285**: 49–69. doi:10.1016/S0022-0981(02)00519-1

Rasmussen, H., and B. B. Jorgensen. 1992. Microelectrode studies of seasonal oxygen-uptake in a coastal sediment - role of molecular-diffusion. Mar. Ecol. Prog. Ser. **81**: 289–303. doi:10.3354/meps081289

Revsbech, N. P. 1989. An oxygen microsensor with a guard cathode. Limnol. Oceanogr. **34**: 474–478. doi:10.4319/lo.1989.34.2.0474

Robertson, E. K., K. L. Roberts, L. D. W. Burdorf, P. Cook, and B. Thamdrup. 2016. Dissimilatory nitrate reduction to ammonium coupled to Fe(II) oxidation in sediments of a periodically hypoxic estuary. Limnol. Oceanogr. **61**: 365–381. doi:10.1002/lno.10220

Rysgaard, S., P. B. Christensen, and L. P. Nielsen. 1995. Seasonal-variation in nitrification and denitrification in estuarine sediment colonized by benthic microalgae and bioturbating infauna. Mar. Ecol. Prog. Ser. **126**: 111–121. doi:10.3354/meps126111

Santner, J., M. Larsen, A. Kreuzeder, and R. N. Glud. 2015. Two decades of chemical imaging of solutes in sediments and soils – a review. Anal. Chim. Acta. **878**: 9–42. doi:10.1016/j.aca.2015.02.006

Seitzinger, S., J. A. Harrison, J. K. Bohlke, A. F. Bouwman, R. Lowrance, B. Peterson, C. Tobias, and G. Van Drecht. 2006. Denitrification across landscapes and waterscapes: A synthesis. Ecol. Appl. **16**: 2064–2090. doi:10.1890/1051-0761(2006)016[2064:DALAWA]2.0.CO;2]

Sloth, N. P., H. Blackburn, L. S. Hansen, N. Risgaard-petersen, and B. A. Lomstein. 1995. Nitrogen Cycling in Sediments with Different Organic Loading. Marine Ecology Progress Series **116**: 163–170.

Stief, P., A. Schramm, D. Altmann, and D. de Beer. 2003. Temporal variation of nitrification rates in experimental freshwater sediments enriched with ammonia or nitrite. FEMS Microbiol. Ecol. **46**: 63–71. doi:10.1016/S0168-6496(03)00193-4

Stief, P., A. Kamp, B. Thamdrup, and R. N. Glud. 2016. Anaerobic nitrogen turnover by sinking diatom aggregates at varying ambient oxygen levels. Front. Microbiol. **7**. doi:10.3389/fmicb.2016.00098

Stocker, R., J. R. Seymour, A. Samadani, D. E. Hunt, and M. F. Polz. 2008. Rapid chemotactic response enables marine bacteria to exploit ephemeral microscale nutrient patches. Proc. Natl. Acad. Sci. USA **105**: 4209–4214. doi:10.1073/pnas.0709765105

Thornton, D. C. O. 2002. Diatom aggregation in the sea: Mechanisms and ecological implications. Eur. J. Phycol. **37**: 149–161. doi:10.1017/S0967026202003657

Underwood, A. J. 1993. The mechanics of spatially replicated sampling programs to detect environmental impacts in a variable World. Aust. J. Ecol. **18**: 99–116. doi:10.1111/j.1442-9993.1993.tb00437.x

Warembourg, F. R. 1993. 5 - Nitrogen fixation in soil and plant systems A2, p. 127–156. *In* T. Henry Blackburn and R. Knowles [eds.], Nitrogen isotope techniques. Academic Press.

Worner, U., H. Zimmerman-Timm, and H. Kausch. 2000. Succession of protists on estuarine aggregates. Microb. Ecol. **40**: 209–222. doi:10.1007/s002480000051

Yang, F., E. Troncy, M. Francoeur, B. Vinet, P. Vinay, G. Czaika, and G. Blaise. 1997. Effects of reducing reagents and temperature on conversion of nitrite and nitrate to nitric oxide and detection of NO by chemiluminescence. Clin. Chem. **43**: 657–662.

Zumft, W. G. 1997. Cell biology and molecular basis of denitrification. Microbiol. Mol. Biol. R. **61**: 533. doi:10.1002/lipi.19970990603

Acknowledgments

We are thankful to A. Glud for microsensor construction and technical assistance, to L. Bristow, D. H. Skov, and S. Møller for help with sample analysis. A. Treusch, A. S. B. Lundgaard, A. Kamp, and N. Risgaard-Petersen are acknowledged for fruitful discussions. We thank the editor and two anonymous reviewers for helping in improuving the manuscript. This study was financially supported by a reasearch grant "Blokstipendium" from the Villum Foundation awarded to RNG and BT (13881). Furthermore the study was financially supported by European Union's Horizon 2020 research and innovation programme (grant agreement No 669947; HADES-ERC to RNG, and Marie Sklodowska-Curie grant agreement No 656385 to UM); and The Danish National Research Council (FNU; 0602-02276B; 12-125843), BT and RNG.

Conflict of Interest

None declared.

Submitted 08 December 2016
Revised 05 May 2017; 28 June 2017
Accepted 29 June 2017

Associate editor: Mary Scranton